ACS NANO
Cite This: ACS Nano 2017, 11, 10384-10391
www.acsnano.org

ARTICLE

Multiple-Patterning Nanosphere Lithography for Fabricating Periodic Three-Dimensional Hierarchical Nanostructures

Xiaobin Xu,[†,‡] Qing Yang,[†,‡] Natcha Wattanatorn,[†,‡] Chuanzhen Zhao,[†,‡] Naihao Chiang,[†,‡] Steven J. Jonas,[†,§,∥,⊥] and Paul S. Weiss*[,†,‡,#]

[†]California NanoSystems Institute, [‡]Department of Chemistry and Biochemistry, [§]Department of Pediatrics, David Geffen School of Medicine, [∥]Eli and Edythe Broad Center of Regenerative Medicine and Stem Cell Research, [⊥]Children's Discovery and Innovation Institute, and [#]Department of Materials Science and Engineering, University of California, Los Angeles, Los Angeles, California 90095, United States

Supporting Information

ABSTRACT: While three-dimensional (3D) configurable hierarchical nanostructures have wide ranging applications in electronics, biology, and optics, finding scalable approaches remains a challenge. We report a robust and general strategy called multiple-patterning nanosphere lithography (MP-NSL) for the fabrication of periodic 3D hierarchical nanostructures in a highly scalable and tunable manner. This nanofabrication technique exploits the selected and repeated etching of polymer nanospheres that serve as resists and that can be shaped in parallel for each processing step. The application of MP-NSL enables the fabrication of periodic, vertically aligned Si nanotubes at the wafer scale with nanometer-scale control in three dimensions including outer/inner diameters, heights/hole-depths, and pitches. The MP-NSL method was utilized to construct 3D periodic hierarchical hybrid nanostructures such as multilevel solid/hollow nanotowers where the height and diameter of each level of each structure can be configured precisely as well as 3D concentric plasmonic nanodisk/nanorings with tunable optical properties on a variety of substrates.

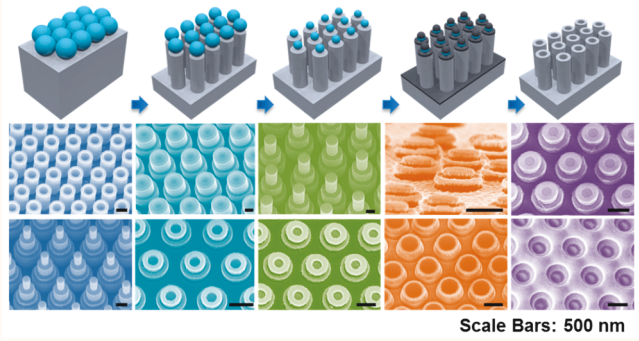

KEYWORDS: *3D lithography, hierarchical nanostructure, multiple patterning, nanostructure, nanotube, nanofabrication, nanosphere lithography*

Periodic semiconductor nanostructures, such as pyramids, holes, wires, pillars, tubes, and cones are increasingly applied in the design of solar cells, biosensors, biomaterials, and drug delivery systems due to their superior optical/electrical properties, biocompatibility, and mechanical properties.[1−10] In particular, periodic single-crystalline silicon (Si) nanotubes[11] assembled *via* electron-beam lithography and nanoimprint lithography demonstrate better light conversion efficiency than other structures in hybrid solar cells, while their biocompatibility[12] and tubular structures also suggest their tantalizing potential as tools to enable improved studies of cellular mechanics,[13−15] circulating tumor cell capture/release,[16] and intracellular biochemical delivery.[17,18] However, despite this interest and their broad applicability, the deployment of periodic Si-nanotube-based devices with controlled dimensions has been limited by the lack of simple and scalable fabrication approaches for these structures.

Current strategies for the fabrication of periodic Si nanostructures, including nanopillars, nanocones, and nanoholes, involve nanosphere lithography,[19−25] because of its low cost, simplicity, and high throughput compared to conventional nanolithographic methods including electron-beam lithography and focused ion-beam milling. Nanosphere lithography employs periodic arrays of self-assembled close-packed mono/bilayer nanospheres (*e.g.*, polystyrene, SiO_2, and others) as masks to pattern underlying substrate materials,[19] However, the fabrication of periodic Si nanotubes with precise dimensional control over large areas remains challenging due primarily to the nanosphere template being used only once during processing. This "*one-time* use" approach restricts traditional nanosphere lithography techniques in that only the

Received: August 1, 2017
Accepted: September 28, 2017
Published: September 28, 2017

DOI: 10.1021/acsnano.7b05472
ACS Nano 2017, 11, 10384−10391

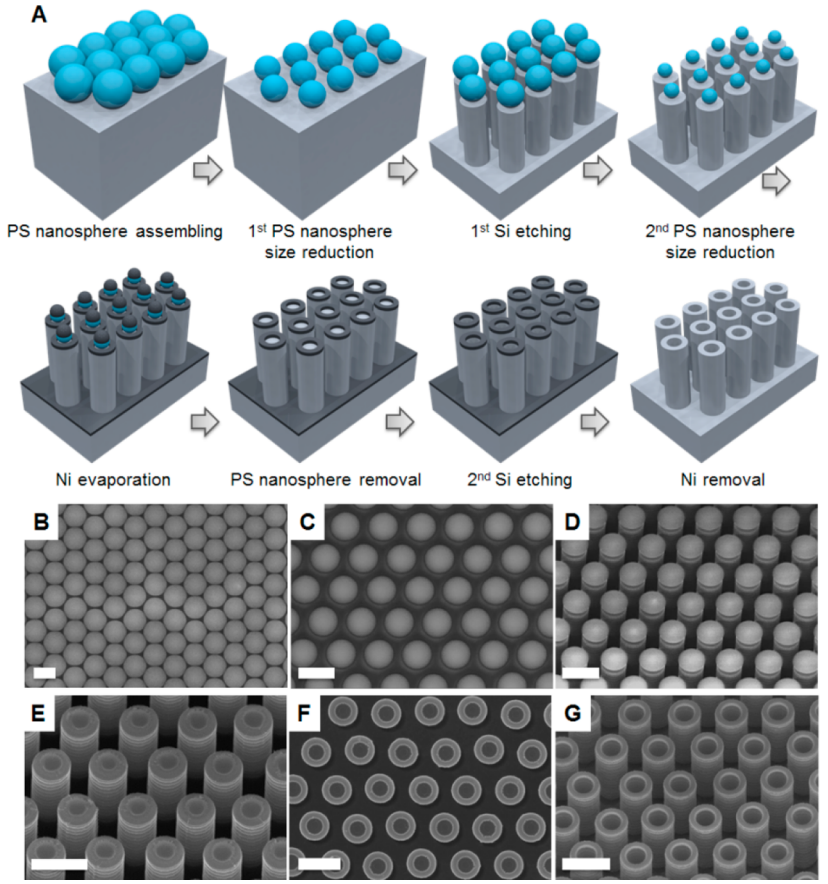

Figure 1. Self-aligned multiple-patterning nanosphere lithography (MP-NSL) for Si nanotube arrays. (A) A schematic illustration of the process. Step 1: A monolayer of close-packed polystyrene (PS) nanospheres is formed at a water/air interface, then transferred onto a Si wafer. The size of the nanospheres defines the ultimate pitches (p) of the Si nanotubes. Step 2: Oxygen plasma RIE reduces the sphere size and defines the outer diameters (d_o) of Si nanotubes. Step 3: Deep reactive ion etching (DRIE) etches Si into nanopillars by using the nanospheres as masks. The outer heights (h_o) of Si nanotubes are controlled by the etch time. Step 4: A second oxygen plasma RIE further reduces the sizes of polymer nanoparticles and defines the inner diameters (d_i) of Si nanotubes. Step 5: Ni is deposited to form Ni nanorings on the Si nanopillars, and it functions as a DRIE mask. Step 6: Polystyrene nanoparticles are removed by 10 min oxygen plasma etching to expose the center part of the Si nanopillars. Step 7: DRIE is performed again to etch holes and to define the hole depth (h_i). Step 8: Ni is removed by HCl, and pristine Si nanotube arrays are obtained. Scanning electron microscope (SEM) images of key intermediates: (B) monolayer of closed-packed polystyrene nanospheres (diameter: 1 μm) formed on a Si wafer; (C) polystyrene nanoparticles on Si wafer after first size reduction; (D) polystyrene nanoparticles on top of periodic Si nanopillar arrays; (E) second size reduction of polystyrene nanoparticles by oxygen plasma (step 4); and (F) Ni nanorings on top of Si nanopillars. The region displayed as dark is Si and the region displayed as bright is Ni. (G) Etching of the inner regions by DRIE to form Si nanotubes (step 7). Images (D, E, G) were taken at a tilt of 30°. Scale bars: 1 μm.

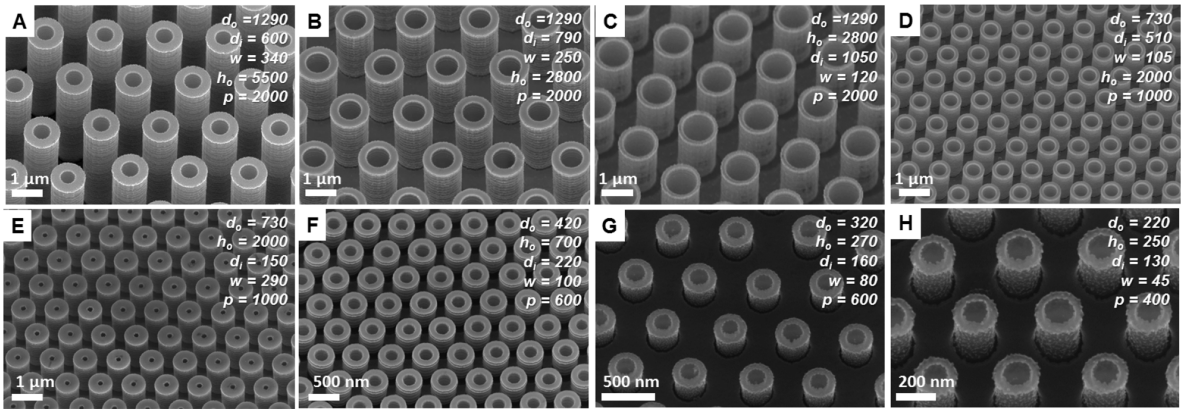

Figure 2. (A–H) Scanning electron micrographs of representative periodic Si nanotube arrays with different parameters in nm: pitch (p), outer diameter (d_o), inner diameter (d_i), sidewall thickness ($w = (d_o - d_i)/2$), and outer height (h_o). Images were recorded at a tilt of 30°. (Units: nm).

DOI: 10.1021/acsnano.7b05472
ACS Nano 2017, 11, 10384–10391

outer diameter of Si nanotubes can be defined fully. For example, previous attempts to generate nanoring-like masks for Si nanotube fabrication lacked suitable control over dimensions (such as tube thickness), quality, and reproducibility.

In this work, we propose and demonstrate a nanosphere lithography strategy named multiple-patterning nanosphere lithography (MP-NSL), which circumvents the limitations of traditional one-time use methods by adopting a multiple use template concept. The MP-NSL method achieves wafer-scale fabrication of periodic Si nanotubes while enabling independent control over all structural dimensions during fabrication including inner/outer tube diameters, heights, hole-depths, and pitches. To our knowledge, this degree of versatility and precision has not previously been reported for structures prepared *via* nanosphere lithography. Moreover, our MP-NSL technique represents a powerful three-dimensional (3D) nanolithographic tool for high-throughput fabrication of periodic hierarchical nanoarchitectures, enabling the assembly of multilevel solid/hollow Si nanotowers and 3D concentric plasmonic nanodisk/nanorings.

RESULTS AND DISCUSSION

The process for fabricating periodic Si nanotubes by MP-NSL is illustrated schematically in Figure 1A with associated scanning electron microscopy (SEM) images of the products from key steps shown in Figure 1B−G. We fabricated a variety of Si nanotube arrays with different parameters: pitches (400 nm to 2 μm), outer heights (100 nm to 6 μm), inner heights (100 nm to 2 μm), outer diameters (220 nm to 1.3 μm), inner diameters (130 to 1050 nm), and tube thicknesses (sub-50 to 500 nm). Representative SEM images of a selection of Si nanotubes are depicted in Figure 2. In addition, SEM images of large area, well-ordered nanosphere templates and Si nanotube arrays with the corresponding Fourier transform patterns are shown in Figures S1 and S2.

The template for MP-NSL consists of a monolayer of polystyrene nanospheres, which is assembled by slowly distributing an aqueous dispersion of the nanospheres drop cast onto a tilted glass slide, as reported elsewhere.[20] The monolayer is then transferred to a 2 cm × 2 cm Si substrate underneath the water/air interface by gently removing the liquid. Note that the pitch of the final Si nanotube arrays is determined by the original diameters of the polystyrene nanosphere template, which can be tailored from several hundred nanometers to several microns depending on their original size. Here, we specifically chose polystyrene nanospheres with diameters of 400 nm, 600 nm, 900 nm, 1 μm, and 2 μm as examples. The assembly of the nanosphere template is highly scalable such that one can easily reach the wafer scale manually and can conceivably reach the square meter scale using automated nanosphere dispensing systems.[26]

Next, the diameters of the polystyrene nanospheres are configured *via* oxygen plasma reactive ion etching (RIE) to define the outer diameter (d_o) of the Si nanotubes. By controlling the oxygen plasma RIE time, one can tailor the nanosphere diameter precisely without changing the pitch. For instance, a 4 min oxygen plasma RIE can uniformly and precisely etch close-packed polystyrene spheres of 1 μm diameter into ∼820 nm diameter nanospheres with identical spacings of ∼180 nm, Figure 1C. As illustrated in Figure 2D and Table 1, the oxygen plasma RIE time and the diameters of polystyrene nanospheres correlate closely, and the results are highly reproducible. The diameters of the nanospheres notably decrease faster with increasing oxygen plasma RIE time due to the polymer nanoparticles becoming flatter with a more oblate ellipsoid shape (Figure S4).[27]

Table 1. Controlling Size Reduction of Polystyrene Nanospheres by Oxygen Plasma RIE

pitch = 1 μm		pitch = 2 μm	
etch time	d_o	etch time	d_o
2.5 min	910 ± 4 nm	4 min	1860 ± 9 nm
3 min	900 ± 4 nm	7 min	1630 ± 8 nm
3.5 min	860 ± 6 nm	10 min	1350 ± 10 nm
4 min	820 ± 5 nm	13 min	1160 ± 9 nm
5 min	760 ± 7 nm	15 min	800 ± 10 nm
6 min	610 ± 7 nm	16 min	740 ± 8 nm
7 min	480 ± 5 nm		
8 min	330 ± 6 nm		

It is important to note that enhancing the adhesion between the polystyrene nanospheres and the underlying Si substrate before dry etching helps to prevent the random tilting of the etched polymer nanoparticles, which could lead to asymmetries in the final pillar/nanotube arrays (Figure S5). The nanospheres were coupled to the Si substrate after the initial oxygen RIE step by heating briefly to 120 °C for ∼30 s. This treatment does not result in noticeable lateral deformation, but appears to fix the etched polymer nanoparticles to prevent moving or tilting during the subsequent processes.

Methods for etching Si involve either wet-etching strategies such as metal-assisted chemical etching[28] or dry-etching approaches such as RIE.[9] Here, we chose a dry etching technique, specifically deep reactive ion etching (DRIE), due to its capability for anisotropic etching, high reproducibility, and nontoxicity. The outer heights (h_o) and inner hole-depths (h_i) of the Si nanotubes are controlled by the DRIE time. Specifically, DRIE *via* the Bosch process, which consists of multiple cycles of passivation and etching, was applied to achieve high-aspect-ratio nanopillars. The alternating cycles of passivation and etching in the Bosch process protect the sidewalls of nanostructures from being etched laterally over large depths. Figure 1D illustrates a typical array of high-aspect-ratio Si nanopillars produced *via* MP-NSL with polystyrene nanoparticles sitting on their tops (h_o = 2000 nm). The Bosch process typically results in periodic "ripples" on the sidewalls as shown in Figure 2, which is called the "scalloping effect". As shown in the high-resolution SEM image in Figure S6, the thickness of the "ripple" is typically ∼25 nm. Note that the top surfaces of the silicon nanopillars remain smooth, as they were protected by the PS bead template during etching. However, the "scalloping effect" can be minimized and/or eliminated in MP-NSL by using an optimized Bosch process[29] or cryogenic-DRIE[30] to generate Si nanostructures with smooth sidewalls. In the present study, low-aspect-ratio Si nanostructures with smooth sidewalls were achieved straightforwardly *via* single-step DRIE, which uses C_4F_8 and SF_6 simultaneously as the etching and passivation gases (Figures 2G,H and S7).

After the fabrication of Si nanopillars, a second oxygen plasma RIE was applied to reduce the size of the polystyrene nanoparticles sitting on top of the pillars (Figure 1D). The smaller nanospheres remain centered on the pillars and serve as templates for subsequent etching treatments to obtain nanotubes. Next, a thin layer of nickel (Ni) was deposited *via* electron-beam evaporation along the exposed Si at the tops of the nanopillars to avoid undesired etching. Nickel was selected

DOI: 10.1021/acsnano.7b05472
ACS Nano 2017, 11, 10384−10391

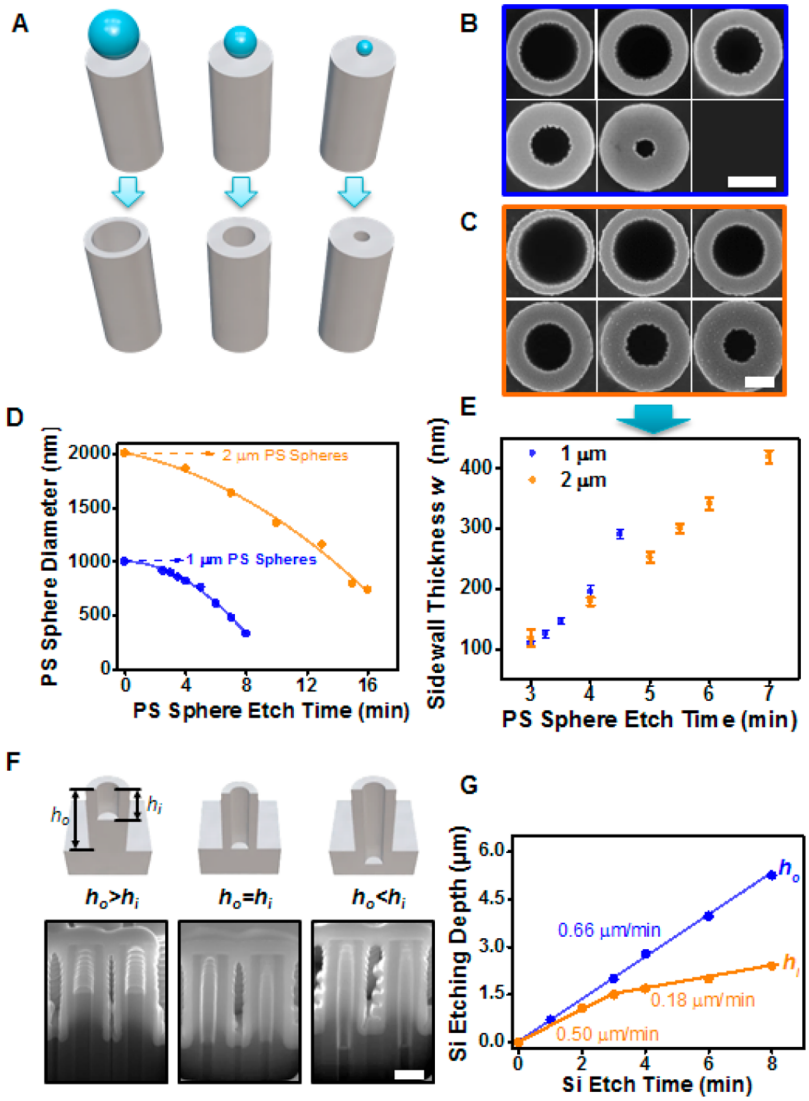

Figure 3. (A) Schematic illustration of tuning the outer and inner diameters (d_o and d_i, respectively) of Si nanotubes. (B) Top-view SEM images of Si nanotubes fabricated from 1 μm polystyrene nanospheres with d_o = 730 ± 7 nm, and sidewall width ($w = (d_o - d_i)/2$) from 105 ± 5 nm to 290 ± 7 nm (scale bar: 400 nm). (C) Top-view SEM images of Si nanotubes fabricated from 2 μm polystyrene (PS) nanospheres with d_o = 1340 ± 12 nm, and w from 120 ± 12 nm to 420 ± 8 nm (scale bar: 400 nm). (D) Oxygen plasma reactive ion etching (RIE) time-dependent size reduction of polystyrene nanoparticles. (E) Oxygen plasma RIE time dependent w corresponding to (B,C) with d_o = 1340 ± 12 nm. (F) Schematic illustrations of independent control of h_o and h_i. From left to right, $h_o > h_i$, $h_o = h_i$, and $h_o < h_i$. Bottom: SEM images of corresponding Si nanotube cross sections prepared by focused ion-beam milling with Pt (white part) as protection layer (scale bar: 500 nm). (G) Plot of DRIE time dependence of h_o and h_i. Si etch rates were 0.66 μm/min for h_o and 0.50 μm/min (0−3 min)/ 0.18 μm/min (3−8 min) for h_i, respectively.

as the masking material as it is highly resistant to Si dry etching processes. The thin Ni layer, typically 20 nm, forms Ni nanorings at the top of the nanopillars and also covers the bottom surface of the Si substrate, Figure 1E. The polymer nanoparticles are subsequently removed with tape to expose the centers of the Si pillars for etching Figure 1F. The inner diameters of the Ni nanorings define the inner diameter (d_i) and sidewall thickness ($w = d_o - d_i$) of nanotubes generated after a second round of DRIE. The Ni is then removed *via* a chemical etch treatment (5% HCl) to obtain the final Si nanotube arrays (Figure 1G).

As illustrated in Figure 3A, altering the time of the second oxygen plasma RIE step enables the inner diameter d_i and thus the sidewall thickness w of the Si nanotubes to be tuned precisely. As a proof of concept, we fabricated a series of Si nanotubes by using 1 and 2 μm polystyrene spheres as masks for MP-NSL. We first fabricated Si nanopillars with diameters of 730 ± 7 nm and 1340 ± 12 nm using the 1 and 2 μm polystyrene spheres masks, respectively. Then, we varied the second oxygen plasma RIE time to control the diameter of the polystyrene nanoparticles on top of the Si nanopillars and applied a second DRIE treatment as described above to generate ordered Si nanotubes with different sidewall thicknesses. As shown in the Tables 1 and 2: For Si nanopillars with d_o = 720 nm, a second oxygen plasma RIE time of 3, 3.25, 3.5, 4, and 4.5 min, resulted in sidewall thicknesses of 105 ± 5, 120 ± 4, 150 ± 5, 200 ± 5, and 290 ± 7 nm, respectively, while for 1340 ± 12 nm diameter Si nanopillars, oxygen plasma RIE times of 3−7 min resulted sidewall thicknesses ranging from 120 ± 12 to 420 ± 8 nm. Even smaller sidewall thickness, such

DOI: 10.1021/acsnano.7b05472
ACS Nano 2017, 11, 10384−10391

Table 2. Controlling Sidewall Thicknesses (w) of Si Nanotubes by Varying the Etch Time Difference between Two Oxygen Plasma RIE

pitch = 1 μm		pitch = 2 μm	
etch time	w	etch time	w
3 min	105 ± 5 nm	3 min	120 ± 12 nm
3.25 min	120 ± 5 nm	4 min	180 ± 7 nm
3.5 min	150 ± 5 nm	5 min	250 ± 8 nm
4 min	200 ± 9 nm	5.5 min	300 ± 8 nm
4.5 min	290 ± 7 nm	6 min	340 ± 9 nm
		7 min	420 ± 8 nm

as 45 ± 2, 80 ± 2, 100 ± 3 nm, can be achieved by further decreasing the RIE time difference, see Figure 2F–H. Such high accuracy control over the nanosphere size is comparable to many electron- or ion-beam-based nanolithographies.

The outer height (h_o) and inner hole-depth (h_i) of the Si nanotubes can be controlled independently by varying their respective DRIE times. The SEM cross-sectional images shown in Figure 3F illustrate three representative Si nanotube arrays with different h_o/h_i ratios, where from left to the right, $h_o > h_i$, $h_o = h_i$ (center), and $h_o < h_i$. The DRIE etching rates used for each h_o and h_i are shown in Figure 3G and Table 3. Specifically,

Table 3. Tuning the Outer/Inner Heights (h_o/h_i) of Si Nanotubes by Controlling the Duration of Deep Reactive Ion Etching

etch time	h_o	etch time	h_i
1 min	700 ± 25 nm	2 min	1100 ± 20 nm
3 min	2000 ± 28 nm	3 min	1500 ± 25 nm
4 min	2800 ± 32 nm	4 min	1700 ± 30 nm
6 min	4000 ± 38 nm	6 min	2000 ± 20 nm
8 min	5200 ± 50 nm	8 min	2410 ± 28 nm

an etch rate of 0.66 μm/min was used for h_o, while rates of 0.50 μm/min (0–3 min) and 0.18 μm/min (3–8 min) were used for h_i. A slower etch rate is observed for h_i, which is known as "RIE lag", that is, the etching rate is related to the feature size, and the smaller the feature size, the lower the etching rate.[31]

The robust and rapid fabrication of periodic 3D hierarchical nanostructures is highly desirable for applications in nanophotonics, metamaterials, and biotechnology.[32] Direct writing fabrication strategies based on two-photon,[33] focused ion-beam, or electron-beam[34] techniques have been developed to assemble 3D hierarchical micro/nanostructures serially, but their widespread use within these areas has been precluded by low fabrication throughputs and a limited selection of compatible materials.

We find that MP-NSL can serve as a high-throughput 3D nanolithographic tool to fabricate a variety of periodic 3D hierarchical nanostructures. For example, as shown in Figure 4A, multilevel Si nanopillars or "nanotowers" with two, three, and four levels were fabricated by reducing the polystyrene nanosphere size twice, three, and four times, respectively, with Si etching applied after each size reduction. A high-resolution SEM image (Figure S6) of multilevel silicon nanotowers shows all the levels have smooth surfaces. The smallest diameters at the apex of the Si nanotowers achieved so far are ~100 nm when using 900 nm nanospheres templates. The sidewall thickness (w) and height (h) of *each* level were controlled individually and precisely by varying the oxygen plasma RIE and DRIE times during processing (Figure 4A). In principle, there is no limitation to the complexity of the nanostructures generated *via* MP-NSL. Potential applications for these multilevel nanotowers include nanobarcodes[35] and antireflective coatings.[36] It is also possible to fabricate hollow Si nanotowers by integrating the etching processes used to generate Si nanotubes above. Moreover, we have applied MP-NSL to pattern similar nanotowers with a wide range of materials, including SiO_2, and have used the nanostructures as a mold for soft materials, such as polydimethylsiloxane (PDMS) (Figure 4A).[37−39]

Plasmonic nanostructures have attracted broad interest, including for potential applications ranging from biosensing and surface-enhanced spectroscopy to optical trapping.[40−46] So far, most plasmonic nanostructures fabricated by nanolithography have been largely two-dimensional. Our 3D nanostructures can further serve as templates for achieving periodic 3D hierarchical plasmonic nanostructures, important for engineering nanophotonics in 3D.[47−49] Simply by evaporating a layer of a plasmonic metal (*e.g.*, gold, silver, aluminum), onto an array of periodic Si/SiO_2/PDMS nanotowers, we obtained periodic 3D plasmonic nanostructures (Figure 4A). After Au evaporation, high-resolution SEM imaging reveals that each layer of the nanotower structures is smooth (Figure S8). The dimensions of these Au nanorings and Au nanodisks as well as the relative vertical distances between them are fully tunable with sub-20 nm-scale resolution, which presents the tantalizing possibility to design and to manipulate the optical properties of these periodic 3D plasmonic nanostructures. For example, we evaporated 50 nm of Au on two slightly different two-level Si nanotowers as shown in Figure 4B, and fully tunable 3D ring/disk plasmonic nanocavities were thereby fabricated. As shown in the reflection spectra of these vertically stacked plasmonic nanostructures, multiple resonant peaks ranged from visible to mid-IR were observed. The reflection spectra agree well with finite-difference-time-domain (FDTD) simulations. The simulation results indicate that multiple peaks and dips result from multimodal plasmonic resonances through hybridization between different plasmonic multipole modes of ring and disk cavities vertically (FDTD simulations of the electric-field and charge distributions are provided in Figure S9). Slight, intentional geometry differences between the two plasmonic nanostructures (sample i *vs* sample ii) result in shifts in the reflection spectra due to changes of the resonance (Figure 4B). Thus, MP-NSL is a tool to design and to fabricate optically tunable 3D plasmonic nanostructures.

CONCLUSIONS AND PROSPECTS

Our results suggest that MP-NSL is a promising 3D nanolithographic tool to achieve a variety of periodic 3D hierarchical nanostructures that can be configured to enable applications in nanophotonics, optoelectronics, electronics, metamaterials, and biotechnology. This strategy is compatible with and could be integrated into micro/nanoscale device manufacturing to add components with functions enabled by rationally designed 3D nanostructures. Additionally, by using beads with different physicochemical properties and/or geometries, even greater control can be achieved.

MATERIALS AND METHODS

Materials. Prime quality 4 in. Si (100) wafers (P/B, 1–10 ohm·cm resistivity) were purchased from University Wafer Inc. (Boston, MA, USA). All polystyrene spheres (1% solids, 400 nm to 2 μm) were

DOI: 10.1021/acsnano.7b05472
ACS Nano 2017, 11, 10384–10391

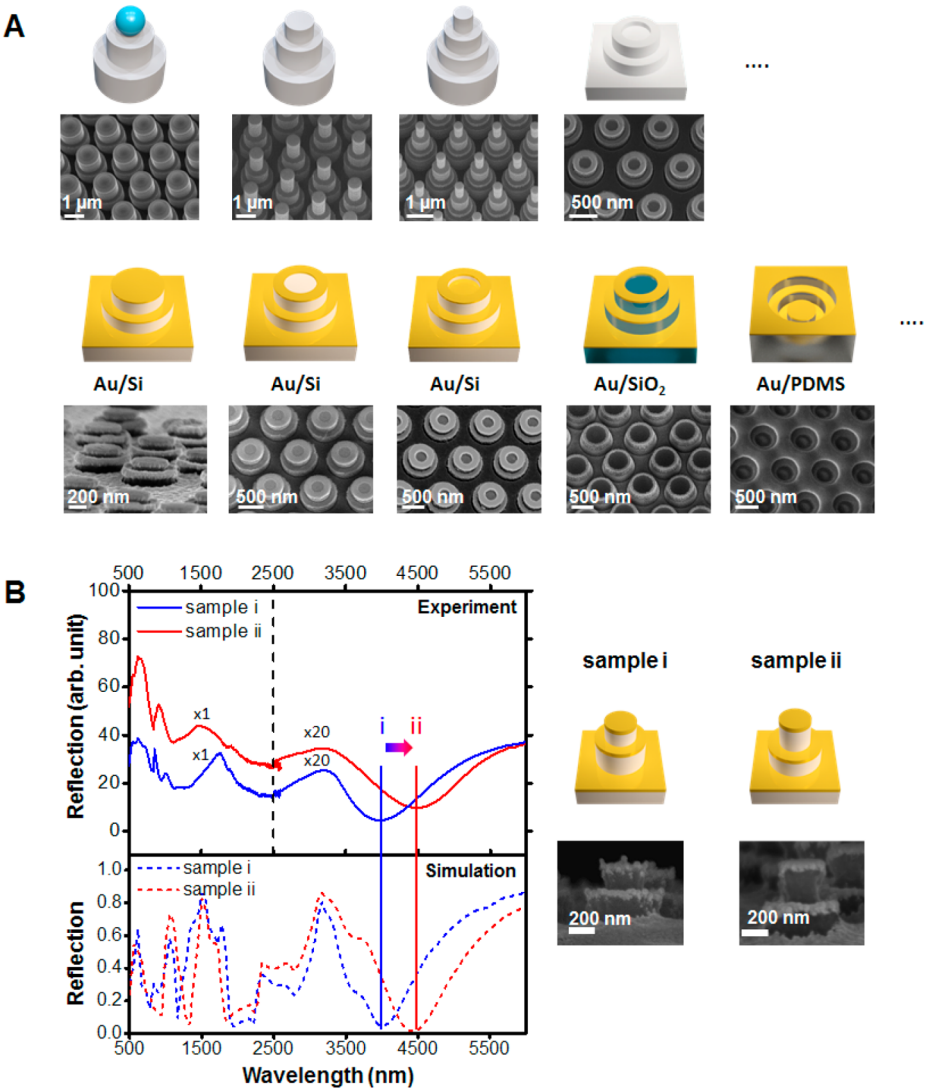

Figure 4. (A) By using multiple-patterning nanosphere lithography, a variety of periodic hierarchical nanostructures have been designed and fabricated: Si nanotowers with two levels, three levels, and four levels with tunable heights (including negative heights for selected levels) and diameters for each level; configurable concentric plasmonic Au nanorings/nanodisk on Si substrates (solid/hollow two-level nanotowers), SiO_2 nanostructures (two-level nanotowers), and flexible polydimethylsiloxane (PDMS) substrates (negatively replicated hollow nanotowers). (B) Reflection visible-infrared spectra of Au/Si nanotowers with different dimensions. Solid lines are the experiment results, and dotted lines are corresponding simulation results. (Sample sizes in nm, sample i: p = 900, d_1 = 530, h_1 = 300, d_2 = 320, h_2 = 230, and t_{Au} = 50; Sample ii: p = 900, d_1 = 570, h_1 = 230, d_2 = 320, h_2 = 300, and t_{Au} = 50). Note that the spectra (500 to 6000 nm) were collected using two different spectrometers with different ranges (500−2500 nm and 2500−6000 nm, respectively) and stitched together at 2500 nm for comparison to simulations (see detailed description in the Supporting Information).

purchased from Thermo Fisher Scientific Inc. (Fremont, CA, USA). Sodium dodecyl sulfate (SDS, 98%) was purchased from Sigma-Aldrich (St. Louis, MO, USA). Hydrochloric acid (36.5 to 38.0% w/w) was purchased from Fisher Scientific Inc. (Fair Lawn, NJ, USA). Evaporation materials including gold (99.99%) and nickel (99.995%) were purchased from K. J. Lesker Company (Jefferson Hills, PA, USA).

Morphology Characterization. The scanning electron micrographs were taken by a Zeiss Supra 40VP scanning electron microscope. Focused ion-beam samples were made and imaged using the Nova 600 SEM/FIB system.

Polystyrene Sphere Monolayer Formation on Si Substrates. The polystyrene nanospheres (1% solids) stock dispersion were centrifuged and redispersed in water/ethanol mixture (1:1 ratio) with 2−4% solids. A 2 cm × 2 cm Si substrate and a 22 mm × 22 mm glass coverslip were treated in an oxygen plasma (Harrick Plasma, Ithaca, NY) for 1 min to generate hydrophilic surfaces. Next, the Si substrate was put in a 2 in. Petri dish, ∼4 mL water was added to immerse the Si substrate fully, and then ∼50 μL 1 wt % SDS was added. The polystyrene nanosphere dispersion in water/ethanol was slowly added to the water/air interface through a tilted glass coverslip that was placed against the edge of the Petri dish to form close-packed monolayers. Then, the water was removed to transfer the polystyrene nanosphere monolayers to the surface of Si substrate. Finally the Si substrate was dried in a vacuum desiccator.

Oxygen Plasma RIE of Polystyrene Nanospheres. An Oxford 80 Plus system was used to tailor the size of polystyrene nanospheres. A time-controlled etching process of the polystyrene nanospheres was carried out under a gas mixture of O_2 (35 sccm) and Ar (10 sccm) at a pressure of 60 mTorr and radio frequency power of 60 W. The polystyrene-nanosphere-coated Si substrate was heated at 120 °C for ∼30 s to fix nanospheres on the Si substrate.

Deep Reactive Ion Etching of Silicon. (1) Bosch process: An inductively coupled plasma reactive ion etcher (ICP-RIE, Plasma Therm SLR700) was used. It involved alternate cycles of passivation and etching steps. During the passivation step, a flow of 24 sccm C_4F_8

DOI: 10.1021/acsnano.7b05472
ACS Nano 2017, 11, 10384−10391

and 12 sccm Ar was used at power of 825 W. During the etching step, a flow of 30 sccm SF_6 and 12 sccm Ar was used at a power of 825 W. (2) Single-step dry etching: The single-step RIE of silicon was completed in a simultaneous flow of 24 sccm C_4F_8, 21 sccm SF_6, and 5 sccm Ar at a pressure of 12 mTorr with ICP power of 650 W and platen power of 9 W (STS Advanced Oxide Etcher) to achieve silicon pillars/tubes with smooth sidewalls. For both processes, the etching depth of Si was controlled by the etching time.

Fabrication of SiO_2 Hierarchical Nanostructures. SiO_2/Si (500-nm-thick SiO_2) substrates with polystyrene nanoparticles as the masks were etched by an Oxford 80 Plus using a gas mixture of CHF_3 (25 sccm) and Ar (25 sccm) at 35 mTorr to generate the SiO_2 hierarchical nanostructures.

Pattern Replication to PDMS Substrates. A 10:1 mass ratio of Sylgard 184 elastomer silicone elastomer base and curing agent were thoroughly mixed and then degassed in a vacuum desiccator. This mixture was poured onto the Si mold with hierarchical nanostructures and cured overnight at 65 °C. After curing, PDMS stamps were carefully removed from the Si mold.

Metal Coating. Desirable substrates were loaded into the vacuum chamber of an electron-beam metal evaporator (Kurt J. Lesker Company, Jefferson Hills, PA) and held at a base pressure of 1×10^{-7} Torr. Ni film was deposited at rate of ∼1 Å/s, and Au film was deposited at rate of ∼0.5 Å/s.

ASSOCIATED CONTENT

Supporting Information

The Supporting Information is available free of charge on the ACS Publications website at DOI: 10.1021/acsnano.7b05472.

Figures (S1−S9) and experimental details describe the characterization of reflection spectra, scanning electron microscope images of periodic nanostructures (polystyrene spheres, silicon nanotubes, oblate ellipsoid shaped polystyrene spheres, asymmetric silicon pillars, silicon nanopillars with smooth sidewalls), large-scale images of silicon nanostructures with corresponding Fourier transforms, high-resolution SEM images, and optical simulations of plasmonic hierarchical nanostructures (PDF)

AUTHOR INFORMATION

Corresponding Author

*E-mail: psw@cnsi.ucla.edu.

ORCID

Xiaobin Xu: 0000-0002-3479-0130
Qing Yang: 0000-0003-4422-5300
Chuanzhen Zhao: 0000-0003-0162-1231
Naihao Chiang: 0000-0003-3782-6546
Steven J. Jonas: 0000-0002-8111-0249
Paul S. Weiss: 0000-0001-5527-6248

Author Contributions

The experiments were designed by all authors, conducted by X.X., Q.Y., N.W., and C.Z., and analyzed by all authors. X.X. and N.C. designed and carried out the simulations. The manuscript was written and edited by all authors.

Notes

The authors declare no competing financial interest.

ACKNOWLEDGMENTS

We gratefully acknowledge support from the National Science Foundation grant no. CMMI-1636136. C.Z. thanks the China Scholarship Council for the CSC-UCLA scholarship. N.W. thanks the Royal Thai Government for the graduate fellowship. S.J.J. acknowledges the support of the Eli and Edythe Broad Center of Regenerative Medicine and Stem Cell Research at UCLA Training Program through its Clinical Fellowship Training Award Program as well as Young Investigator Award funds from the Hyundai Hope on Wheels Foundation and the Alex's Lemonade Stand Foundation for Pediatric Cancer Research. P.S.W. and S.J.J. also wish to acknowledge the David Geffen School of Medicine and Eli and Edythe Broad Center of Regenerative Medicine and Stem Cell Research at UCLA for seed funding. We acknowledge the facilities and thank the staff of the Electron Imaging Center, Integrated Systems Nanofabrication Cleanroom of the UCLA California NanoSystems Institute, and NanoLab at UCLA, especially Dr. Tom Lee.

REFERENCES

(1) Kim, Y. Y.; Kim, H. J.; Jeong, J. H.; Lee, J.; Choi, J. H.; Jung, J. Y.; Lee, J. H.; Cheng, H.; Lee, K. W.; Choi, D. G. Facile Fabrication of Silicon Nanotube Arrays and Their Application in Lithium-Ion Batteries. *Adv. Eng. Mater.* **2016**, *18*, 1349−1353.

(2) Yoo, J.-K.; Kim, J.; Jung, Y. S.; Kang, K. Scalable Fabrication of Silicon Nanotubes and Their Application to Energy Storage. *Adv. Mater.* **2012**, *24*, 5452−5456.

(3) Park, M.-H.; Kim, M. G.; Joo, J.; Kim, K.; Kim, J.; Ahn, S.; Cui, Y.; Cho, J. Silicon Nanotube Battery Anodes. *Nano Lett.* **2009**, *9*, 3844−3847.

(4) Wu, H.; Chan, G.; Choi, J. W.; Ryu, I.; Yao, Y.; Mcdowell, M. T.; Lee, S. W.; Jackson, A.; Yang, Y.; Hu, L.; Cui, Y. Stable Cycling of Double-Walled Silicon Nanotube Battery Anodes through Solid−Electrolyte Interphase Control. *Nat. Nanotechnol.* **2012**, *7*, 310−315.

(5) Xie, C.; Nie, B.; Zeng, L.; Liang, F.-X.; Wang, M.-Z.; Luo, L.; Feng, M.; Yu, Y.; Wu, C.-Y.; Wu, Y.; Yu, S.-H. Core−Shell Heterojunction of Silicon Nanowire Arrays and Carbon Quantum Dots for Photovoltaic Devices and Self-Driven Photodetectors. *ACS Nano* **2014**, *8*, 4015−4022.

(6) Wei, W.-R.; Tsai, M.-L.; Ho, S.-T.; Tai, S.-H.; Ho, C.-R.; Tsai, S.-H.; Liu, C.-W.; Chung, R.-J.; He, J.-H. Above-11%-Efficiency Organic−Inorganic Hybrid Solar Cells with Omnidirectional Harvesting Characteristics by Employing Hierarchical Photon-Trapping Structures. *Nano Lett.* **2013**, *13*, 3658−3663.

(7) Ali, M.; Zhou, F.; Chen, K.; Kotzur, C.; Xiao, C.; Bourgeois, L.; Zhang, X.; Macfarlane, D. R. Nanostructured Photoelectrochemical Solar Cell for Nitrogen Reduction Using Plasmon-Enhanced Black Silicon. *Nat. Commun.* **2016**, *7*, 11335.

(8) Kelzenberg, M. D.; Boettcher, S. W.; Petykiewicz, J. A.; Turner-Evans, D. B.; Putnam, M. C.; Warren, E. L.; Spurgeon, J. M.; Briggs, R. M.; Lewis, N. S.; Atwater, H. A. Enhanced Absorption and Carrier Collection in Si Wire Arrays for Photovoltaic Applications. *Nat. Mater.* **2010**, *9*, 239−244.

(9) Garnett, E.; Yang, P. Light Trapping in Silicon Nanowire Solar Cells. *Nano Lett.* **2010**, *10*, 1082−1087.

(10) Xu, X.; Liu, C.; Kim, K.; Fan, D. L. Electric-Driven Rotation of Silicon Nanowires and Silicon Nanowire Motors. *Adv. Funct. Mater.* **2014**, *24*, 4843−4850.

(11) Jeong, H.; Song, H.; Pak, Y.; Kwon, I. K.; Jo, K.; Lee, H.; Jung, G. Y. Enhanced Light Absorption of Silicon Nanotube Arrays for Organic/Inorganic Hybrid Solar Cells. *Adv. Mater.* **2014**, *26*, 3445−3450.

(12) Chiappini, C.; De Rosa, E.; Martinez, J. O.; Liu, X.; Steele, J.; Stevens, M. M.; Tasciotti, E. Biodegradable Silicon Nanoneedles Delivering Nucleic Acids Intracellularly Induce Localized *in Vivo* Neovascularization. *Nat. Mater.* **2015**, *14*, 532−539.

(13) Bucaro, M. A.; Vasquez, Y.; Hatton, B. D.; Aizenberg, J. Fine-Tuning the Degree of Stem Cell Polarization and Alignment on Ordered Arrays of High-Aspect-Ratio Nanopillars. *ACS Nano* **2012**, *6*, 6222−6230.

(14) Polacheck, W. J.; Chen, C. S. Measuring Cell-Generated Forces: A Guide to the Available Tools. *Nat. Methods* **2016**, *13*, 415−423.

DOI: 10.1021/acsnano.7b05472
ACS Nano 2017, 11, 10384−10391

(15) Weng, S. N.; Shao, Y.; Chen, W. Q.; Fu, J. P. Mechanosensitive Subcellular Rheostasis Drives Emergent Single-Cell Mechanical Homeostasis. *Nat. Mater.* **2016**, *15*, 961−967.
(16) Green, B. J.; Saberi Safaei, T.; Mepham, A.; Labib, M.; Mohamadi, R. M.; Kelley, S. O. Beyond the Capture of Circulating Tumor Cells: Next-Generation Devices and Materials. *Angew. Chem., Int. Ed.* **2016**, *55*, 1252−1265.
(17) Fox, C. B.; Cao, Y.; Nemeth, C. L.; Chirra, H. D.; Chevalier, R. W.; Xu, A. M.; Melosh, N. A.; Desai, T. A. Fabrication of Sealed Nanostraw Microdevices for Oral Drug Delivery. *ACS Nano* **2016**, *10*, 5873−5881.
(18) Wu, Y.-C.; Wu, T.-H.; Clemens, D. L.; Lee, B.-Y.; Wen, X.; Horwitz, M. A.; Teitell, M. A.; Chiou, P.-Y. Massively Parallel Delivery of Large Cargo into Mammalian Cells with Light Pulses. *Nat. Methods* **2015**, *12*, 439−444.
(19) Hulteen, J. C.; Van Duyne, R. P. Nanosphere Lithography: A Materials General Fabrication Process for Periodic Particle Array Surfaces. *J. Vac. Sci. Technol., A* **1995**, *13*, 1553−1558.
(20) Chen, K.; Rajeeva, B. B.; Wu, Z.; Rukavina, M.; Dao, T. D.; Ishii, S.; Aono, M.; Nagao, T.; Zheng, Y. Moiré Nanosphere Lithography. *ACS Nano* **2015**, *9*, 6031−6040.
(21) Kosiorek, A.; Kandulski, W.; Glaczynska, H.; Giersig, M. Fabrication of Nanoscale Rings, Dots, and Rods by Combining Shadow Nanosphere Lithography and Annealed Polystyrene Nanosphere Masks. *Small* **2005**, *1*, 439−444.
(22) Haynes, C. L.; Van Duyne, R. P. Nanosphere Lithography: A Versatile Nanofabrication Tool for Studies of Size-Dependent Nanoparticle Optics. *J. Phys. Chem. B* **2001**, *105*, 5599−5611.
(23) Huang, Z.; Fang, H.; Zhu, J. Fabrication of Silicon Nanowire Arrays with Controlled Diameter, Length, and Density. *Adv. Mater.* **2007**, *19*, 744−748.
(24) Jeong, S.; Mcgehee, M. D.; Cui, Y. All-Back-Contact Ultra-Thin Silicon Nanocone Solar Cells with 13.7% Power Conversion Efficiency. *Nat. Commun.* **2013**, *4*, 2950.
(25) Jeong, S.; Garnett, E. C.; Wang, S.; Yu, Z.; Fan, S.; Brongersma, M. L.; Mcgehee, M. D.; Cui, Y. Hybrid Silicon Nanocone−Polymer Solar Cells. *Nano Lett.* **2012**, *12*, 2971−2976.
(26) Gao, P. Q.; He, J.; Zhou, S. Q.; Yang, X.; Li, S. Z.; Sheng, J.; Wang, D.; Yu, T. B.; Ye, J. C.; Cui, Y. Large-Area Nanosphere Self-Assembly by a Micro-Propulsive Injection Method for High Throughput Periodic Surface Nanotexturing. *Nano Lett.* **2015**, *15*, 4591−4598.
(27) Zhang, J.; Li, Y.; Zhang, X.; Yang, B. Colloidal Self-Assembly Meets Nanofabrication: From Two-Dimensional Colloidal Crystals to Nanostructure Arrays. *Adv. Mater.* **2010**, *22*, 4249−4269.
(28) Ge, M.; Rong, J.; Fang, X.; Zhou, C. Porous Doped Silicon Nanowires for Lithium Ion Battery Anode with Long Cycle Life. *Nano Lett.* **2012**, *12*, 2318−2323.
(29) Morton, K. J.; Nieberg, G.; Bai, S.; Chou, S. Y. Wafer-Scale Patterning of Sub-40 nm Diameter and High Aspect Ratio (>50:1) Silicon Pillar Arrays by Nanoimprint and Etching. *Nanotechnology* **2008**, *19*, 345301.
(30) Li, Z.; Chen, Y.; Zhu, X.; Zheng, M.; Dong, F.; Chen, P.; Xu, L.; Chu, W.; Duan, H. Fabrication of Single-Crystal Silicon Nanotubes with Sub-10 nm Walls Using Cryogenic Inductively Coupled Plasma Reactive Ion Etching. *Nanotechnology* **2016**, *27*, 365302.
(31) Chung, C.-K. Geometrical Pattern Effect on Silicon Deep Etching by an Inductively Coupled Plasma System. *J. Micromech. Microeng.* **2004**, *14*, 656−662.
(32) Fan, Z.; Razavi, H.; Do, J.-W.; Moriwaki, A.; Ergen, O.; Chueh, Y.-L.; Leu, P. W.; Ho, J. C.; Takahashi, T.; Reichertz, L. A.; Neale, S.; Yu, K.; Wu, M.; Ager, J. W.; Javey, A. Three-Dimensional Nanopillar-Array Photovoltaics on Low-Cost and Flexible Substrates. *Nat. Mater.* **2009**, *8*, 648−653.
(33) Perry, J. W.; Cumpston, B. H.; Ananthavel, S. P.; Barlow, S.; Dyer, D. L.; Ehrlich, J. E.; Erskine, L. L.; Heikal, A. A.; Kuebler, S. M.; Lee, I. Y. S.; Mccord-Maughon, D.; Qin, J.; Röckel, H.; Rumi, M.; Wu, X.-L.; Marder, S. R. Two-Photon Polymerization Initiators for Three-Dimensional Optical Data Storage and Microfabrication. *Nature* **1999**, *398*, 51−54.
(34) Yamazaki, K.; Yamaguchi, H. Flexible Nanofabrication in Three-Dimensional Electron-Beam Lithography Enhanced by Suppression of Proximity Effect. *Appl. Phys. Express* **2008**, *1*, 097001.
(35) Qin, L.; Banholzer, M. J.; Millstone, J. E.; Mirkin, C. A. Nanodisk Codes. *Nano Lett.* **2007**, *7*, 3849−3853.
(36) Raut, H. K.; Ganesh, V. A.; Nair, A. S.; Ramakrishna, S. Anti-Reflective Coatings: A Critical, in-Depth Review. *Energy Environ. Sci.* **2011**, *4*, 3779−3804.
(37) Cao, H. H.; Nakatsuka, N.; Liao, W.-S.; Serino, A. C.; Cheunkar, S.; Yang, H.; Weiss, P. S.; Andrews, A. M. Advancing Biocapture Substrates *via* Chemical Lift-Off Lithography. *Chem. Mater.* **2017**, *29*, 6829.
(38) Xu, X.; Yang, Q.; Cheung, K. M.; Zhao, C.; Wattanatorn, N.; Belling, J. N.; Abendroth, J. M.; Slaughter, L. S.; Mirkin, C. A.; Andrews, A. M.; Weiss, P. S. Polymer-Pen Chemical Lift-Off Lithography. *Nano Lett.* **2017**, *17*, 3302−3311.
(39) Liao, W.-S.; Cheunkar, S.; Cao, H. H.; Bednar, H. R.; Weiss, P. S.; Andrews, A. M. Subtractive Patterning *via* Chemical Lift-Off Lithography. *Science* **2012**, *337*, 1517−1521.
(40) Brolo, A. G. Plasmonics for Future Biosensors. *Nat. Photonics* **2012**, *6*, 709−713.
(41) Juan, M. L.; Righini, M.; Quidant, R. Plasmon Nano-Optical Tweezers. *Nat. Photonics* **2011**, *5*, 349−356.
(42) Lu, Y. J.; Kim, J.; Chen, H. Y.; Wu, C.; Dabidian, N.; Sanders, C. E.; Wang, C. Y.; Lu, M. Y.; Li, B. H.; Qiu, X.; Chang, W. H.; Chen, L. J.; Shvets, G.; Shih, C. K.; Gwo, S. Plasmonic Nanolaser Using Epitaxially Grown Silver Film. *Science* **2012**, *337*, 450−453.
(43) Nie, S. Probing Single Molecules and Single Nanoparticles by Surface-Enhanced Raman Scattering. *Science* **1997**, *275*, 1102−1106.
(44) Rodrigo, D.; Limaj, O.; Janner, D.; Etezadi, D.; Garcia De Abajo, F. J.; Pruneri, V.; Altug, H. Mid-Infrared Plasmonic Biosensing with Graphene. *Science* **2015**, *349*, 165−168.
(45) Xu, X.; Li, H.; Hasan, D.; Ruoff, R. S.; Wang, A. X.; Fan, D. L. Near-Field Enhanced Plasmonic-Magnetic Bifunctional Nanotubes for Single Cell Bioanalysis. *Adv. Funct. Mater.* **2013**, *23*, 4332−4338.
(46) Zheng, Y. B.; Payton, J. L.; Chung, C.-H.; Liu, R.; Cheunkar, S.; Pathem, B. K.; Yang, Y.; Jensen, L.; Weiss, P. S. Surface-Enhanced Raman Spectroscopy to Probe Reversibly Photoswitchable Azobenzene in Controlled Nanoscale Environments. *Nano Lett.* **2011**, *11*, 3447−3452.
(47) Kuzyk, A.; Schreiber, R.; Zhang, H.; Govorov, A. O.; Liedl, T.; Liu, N. Reconfigurable 3D Plasmonic Metamolecules. *Nat. Mater.* **2014**, *13*, 862−866.
(48) Frank, B.; Yin, X.; Schäferling, M.; Zhao, J.; Hein, S. M.; Braun, P. V.; Giessen, H. Large-Area 3D Chiral Plasmonic Structures. *ACS Nano* **2013**, *7*, 6321−6329.
(49) De Angelis, F.; Malerba, M.; Patrini, M.; Miele, E.; Das, G.; Toma, A.; Zaccaria, R. P.; Di Fabrizio, E. 3D Hollow Nanostructures as Building Blocks for Multifunctional Plasmonics. *Nano Lett.* **2013**, *13*, 3553−3558.

DOI: 10.1021/acsnano.7b05472
ACS Nano 2017, 11, 10384−10391